Density Fluctuation of the Amorphous Region of Poly(ethylene terephthalate) Films by Quasi-Spinodal Decomposition

Tong Xu, Yuezhen Bin, Yuko Nakagaki, and Masaru Matsuo*

Department of Textile and Apparel Science, Faculty of Human Life and Environment, Nara Women's University, Nara 630-8263, Japan

Received July 30, 2003; Revised Manuscript Received November 26, 2003

ABSTRACT: Crystallization of polymers was studied in terms of density fluctuation of amorphous phase by using amorphous poly(ethylene terephthalate) (PET) films in disoriented and oriented states. When the amorphous film was put into a hot oven with desired temperature and an incident beam of He−Ne gas laser was directed to the film, the scattered intensity against time was classified into three regions. In the first stage, the scattered intensity hardly changed. In the second stage, the logarithm of scattered intensity increased linearly. This tendency was apparently in accordance with concentration fluctuation of linear theories of spinodal decomposition (SD) originally proposed by Cahn for small molecules and that modified by de Gennes for the polymer system which describe the initial stage in the phase separation process. In the third stage, the increase in intensity started to deviate from the linear relationship and tended to level off. The scattering maximum increased with time and maintained at the same scattered vector in stage II and then tended to shift toward a lower angle in stage III, characterizing SD. Surprisingly, the above phenomenon indicates that the observation scale of the density fluctuation associated with the driving force of the crystallization process was several thousand nanometers. Such behavior was quite different from the density fluctuation at smaller scales detected by X-ray diffraction and scattering. On the basis of the second stage, the apparent spinodal temperatures (T_s) could be estimated from the dynamics measured as a function of temperature for undrawn and drawn PET films. The growth rate maximum of the density fluctuation was independent of the scattered vector q and increased with annealing temperature. This indicates that the phase separation due to density fluctuation occurs in thermodynamic unstable state and crystallization takes place partially in the higher density region of amorphous chains. This mechanism is different from crystallization associated with nucleation and growth. To demonstrate this concept in detail, further analysis was done by using wide-angle X-ray diffraction, differential scanning calorimetry, and small-angle light scattering under polarization conditions and density measurement.

Introduction

Extensive studies have been performed on the morphology of crystalline polymers obtained by annealing amorphous films or by cooling melt films.[1−8] The growth of polymer crystals has been well established in the literature, and there are reliable theories to predict the kinetics of crystallization. Most of these studies have been concentrated on the observation of crystal growth processes, while little information exists about how nucleation proceeds from the disordered amorphous state. The initiation of crystallization or nucleation step remains somewhat of a mystery.

Recently, there is an increasing body of evidence that polymer crystallization in general may be assisted by the formation on an intermediate metastable state. Geil[9] has reported an amorphous structure having nodules of about 100 Å in diameter in ice water quenched PET which aggregated to form spherilites by transmission electron microscopy. Herglotz[10] has found that crystalline PET films annealed from the glass have a supermolecular structure with a size of about 1000 nm. These experimental results indicate that the long-range structure is formed during the annealing processes of PET.

Apart from the above concept, Imai et al.[8] investigated the kinetics during the induction period of PET crystallization by means of depolarized light scattering. They pointed out that this period is associated with spinodal decomposition (SD) caused by orientation fluctuation of chain segments in terms of the concept concerning the transformation from the isotropic to nematic phase proposed by Doi et al.[11] In their reports, the time evolution of scattering profiles in the induction period reflects the growth process of long-range density fluctuations, and the formation process of the dense region during the induction period is very similar to the spinodal decomposition of phase separation process. They concluded that crystallization begins after this dense region grows to a certain size. The similar analysis was proposed by Teril et al.[12] for oriented and disoriented polypropylene films and by Strobl[13,14] for PET films. Strobl[14] pointed out that oriented PET crystallizes via a spinodal process on the basis of the report that logarithm of SAXS scattered intensity increases linearly against time.

This paper deals with detailed structural formation of disoriented and oriented amorphous PET films when annealing isothermally. The estimation is mainly done in terms of density fluctuation of amorphous chains under annealing process at desired temperature. In doing so, mechanisms and dynamics of the crystallization associated with the structural formation of PET were estimated by depolarized light scattering, small-angle light scattering under H_v cross-polarization, X-ray diffraction intensity, and density as a function of time. To pursue the analysis of the density fluctuation of

* To whom all correspondence should be addressed: Fax 81-742-20-3462; e-mail m-matsuo@cc.nara-un.ac.jp.

10.1021/ma030408r CCC: $27.50
Published on Web 08/06/2004

Table 1. Characteristics of Test Specimens

sample	density (g/cm^3)	crystallinity (%) from density	optical birefringence (Δ)
original sample ($\lambda = 1$)	1.335	0.31	1.0×10^{-4}
100 °C ($\lambda = 2$)	1.336	0.52	4.5×10^{-3}

amorphous phase of PET, the spinodal temperature as well as characteristic parameters was mainly estimated from the dynamics of the linear SD regime detected by a He−Ne gas laser.

Experimental Section

Preparation of Specimens. The PET used in this study was furnished by Toyobo Industries, Inc. The number-average molecular weight ($\bar{M}_n$) was 15 000, and the polydispersity termed as $\bar{M}_w/\bar{M}_n$ was 3.47, where $\bar{M}_w$ is a weight-average molecular weight. The density of the PET film is ca. 1.335 g cm^{-3}, which agrees with the value reported for amorphous PET.[15] The film thickness is about 200 μm. The original (undrawn) film ($\lambda = 1$) was cut into strips of length 70 mm and width 10 mm, and the strips clamped in a manual stretching device were elongated manually up to the draw ratio of $\lambda = 2$ in a hot water bath at 100 °C. This elongation condition was effective to ensure uniform draw and to avoid thermal crystallization. After drawing, the material was put into a cold−water bath quickly to freeze the structural state. The draw ratio was determined in the usual way by measuring the displacement of ink marks placed 2 mm apart on the specimen prior to drawing.

DSC Measurement. The thermal behavior of PET was studied with a differential scanning calorimeter (EXSTAR 6000) of Seiko Instrument Inc. Each film was cut into identical circular shapes and the samples, weighing about 10 mg, were placed in a standard aluminum sample pan. The sample was heated at a scanning 20 °C/min. The measured glass transition temperature of the original film was 72.3 °C.

Crystallinity. The weight crystallinity, X_c, of PET films was calculated from the density measured by a pycnometer in mixture of carbon tetrachloride and *n*-heptane as a medium, using 1.455 and 1.335 g cm^{-3} as the densities of the crystal (ρ_c) and amorphous (ρ_a) phases, respectively.[15]

$$X_c = \frac{\rho_c(\rho - \rho_a)}{\rho(\rho_c - \rho_a)} \times 100\% \quad (1)$$

As listed in Table 1, the crystallinity of the test specimens was ca. 0.3−0.5%. This means that the specimens almost compose of the amorphous phase.

Birefringence Measurement. Birefringence was measured between crossed polars in an optical microscope (Olympus 206648). The values are listed in Table 1.

SALS Measurement. The in-situ time-revolved scattered intensity (depolarization condition) was measured by using a 632.8 nm He−Ne laser. To measure time dependence of scattered intensity, nine photodiodes were set at the desired scattering angle (θ) in order to detect the scattering beam at various angles simultaneously. The specimens were subjected to a rapid temperature jump to desired temperatures. The time required to achieve the equilibrium temperature is ca. 1 min. The change in angular distribution of scattered intensity with time was measured when the fixed specimen was annealed isothermally in a temperature-controlled cell.

Wide-Angle X-ray Diffraction (WAXD) Measurement. The X-ray measurements were carried out with a 12 kW rotating-anode X-ray generator (Rigaku RDA-rA) operated at 200 mA and 40 kV. The intensity was detected with a curved position-sensitive proportional counter (PSPC) in an equatorial direction. The X-ray source was monochromatized to Cu Kα radiation with a platelike graphite monochromator. The scattering intensity with time was measured in the range 5°−35° (twice the Bragg angle, $2\theta_B$).

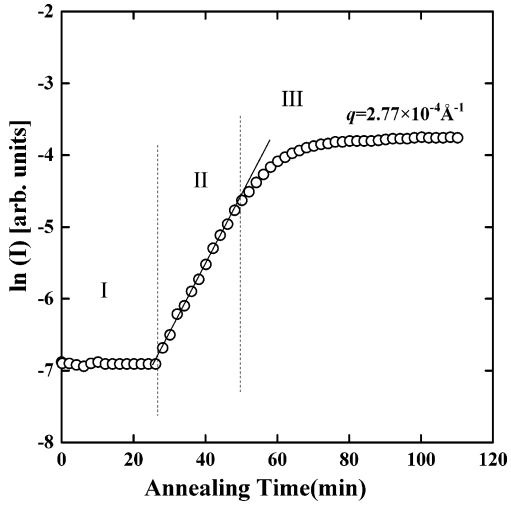

Figure 1. Typical annealing time dependence of logarithm of the scattered intensity at $q = 2.77 \times 10^{-4}$ Å^{-1} measured for undrawn amorphous PET film annealing at 114 °C.

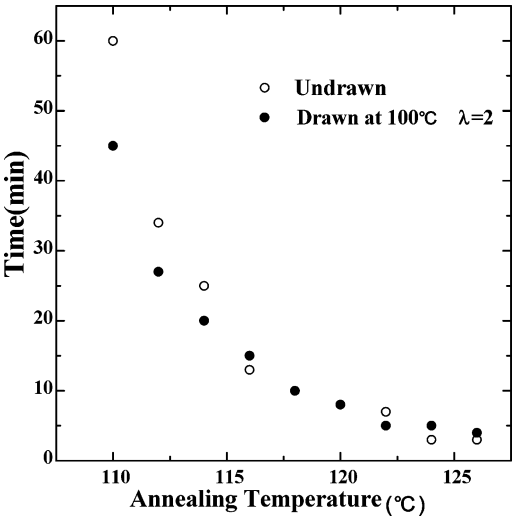

Figure 2. Annealing temperature dependence of the time length of the first stage.

Result and Discussion

Figure 1 shows the typical time dependence of the logarithm of the scattered intensity measured for undrawn amorphous PET film ($\lambda = 1$) annealed at 114 °C. The measurement was carried out at $q = 2.77 \times 10^{-4}$ Å. q is the magnitude of the scattered vector given by $q = (4\pi n/\lambda) \sin(\theta/2)$, with λ, θ, and n being the wavelength of the light in the film, the scattered angle, and the refractive index, respectively. The curve may be classified into three stages: the first stage (stage I) where the scattered intensity hardly changes with time, the second stage (stage II) where the intensity increases linearly, and the third stage (stage III) where the intensity starts to deviate from the linear relationship and tends to levels off. The behavior at stage II is similar to the initial stage of phase separation of isotropic amorphous polymer blends by spinodal decomposition (SD).[16,17]

Figure 2 shows the length of stage I at the indicated annealing temperatures measured for undrawn ($\lambda = 1$) and drawn ($\lambda = 2$) films. The length of stage I is

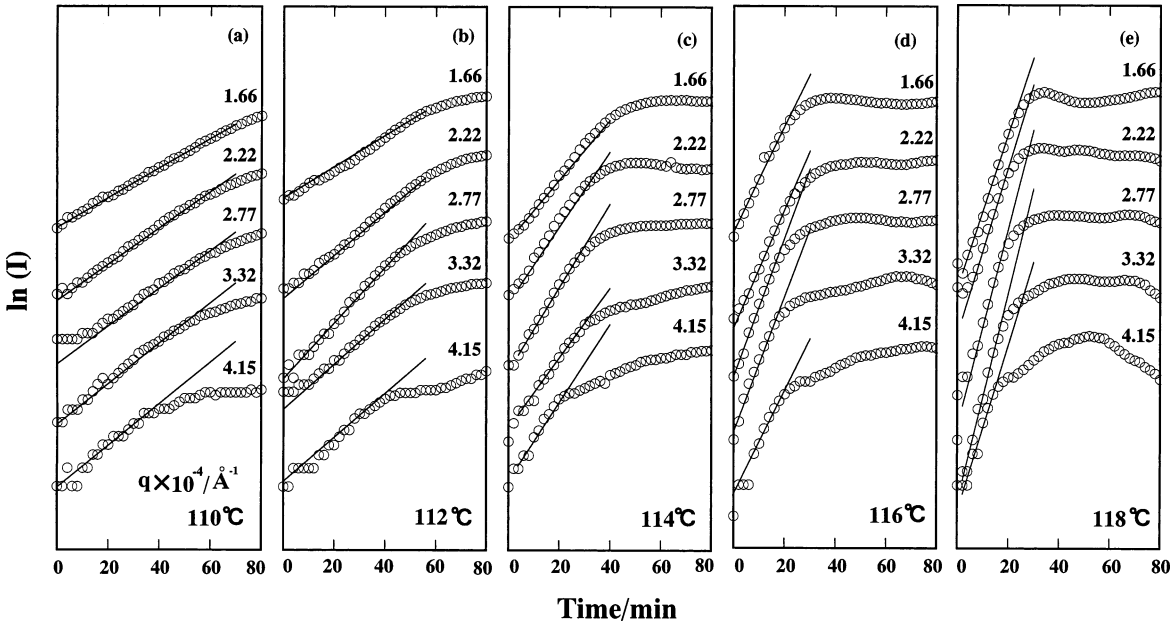

Figure 3. Logarithm plots of the scattered intensity against time at various q after the initiation of spinodal decomposition observed for amorphous PET films. The specimens were annealed at the indicated temperature.

dependent upon the annealing temperature and elongation. It has been reported that stage I may correspond to a limited time scale when the average length of rigid segments attains a critical value given by a Shimada, Doi, and Okano theory[18] and is assigned as a process where the polymer chain segments begin to partially change the conformation. As for PET, it has been reported[7,19] that the internal rotation of ethylene groups begins to be allowed due to the release from the frozen state, and the trans form is preferred to the gauche one to ensure a more stable state when the amorphous film was annealed above the glass transition temperature. We speculated that in stage I the conformational changes and the lengths of the rigid segments of polymer chains increase. However, the density fluctuation hardly occurs in this stage since the scattered intensity hardly increases in this stage. This means that in the stage I the average length of the rigid segments do not attain a critical value. When the critical length is achieved, the isotropic amorphous state becomes unstable, indicating that density fluctuation occurs by spinodal decomposition. However, Matsuba et al.[20,21] also pointed out that on stage I (the very early stage) the intensity of the IR band originated from noncrystalline trans conformation hardly increases[21] for poly(ethylene naphthalate) (PEN). Incidentally, the time lengths of stage I decreased with increasing annealing temperature and the birefringence by elongation (see Table 1). When the annealing temperatures were higher than ca. 116 °C, the interval of stage I for the undrawn and drawn ($\lambda = 2$) films tended to close to the same time value.

Figures 3 and 4 show typically time evolution of the scattered light intensity at various q. The initial plot (0 min) in all curves corresponds to the starting point of stage II. The samples were isothermally annealed at the indicated temperature. The temperature dependence of the refractive index could be neglected within the experimental error in the given temperature range. The observed time evolution of the scattering profiles during the stage II is very similar to the results observed for spinodal decomposition type of phase separation in blend systems.[22,23] A similar phenomenon was reported for the annealing process of PET using the time-resolved SAXS method.[24,25] The linear increasing relationship shown in Figures 3 and 4 in stage II is also similar to the behavior associated with the linear theory of the initial stage of spinodal decomposition proposed by Cahn,[26,27] although the present system is only one component, different from the phase separation of two components like blend films and gels (polymer and solvent). If this behavior detected by a He−Ne gas laser with a wavelength longer than 600 nm is caused by density fluctuation of amorphous chains, this concept must be out of the framework for the appearance of crystal nuclei. If this concept is correct, the linear increase must be independent of crystalline nucleation. If the behaviors in Figures 3 and 4 are due to the density fluctuation of amorphous region to dissolve thermodynamically unstable state arisen by rapid jump of temperature, we must emphasize again that stage II must be independent of the formation of crystal nuclei. To check this, DSC, X-ray diffraction, density, and SALS were measured. The detailed analysis of these measurements shall be discussed in the following.

Figure 5 shows the DSC curves of undrawn and drawn PET films. The heating rate is 20 °C/min. Such rapid heating rate was used to follow the rapid jump of temperature in the SALS experiment. Each melting endotherm appeared as a single peak at around 257 °C is independent of the draw ratio, but the position and the shape of exothermic peak associated with thermal crystallization depend on the draw ratio. Namely, the exothermic peak of the specimen with $\lambda = 2$ shifts to lower temperature side and becomes smaller with increasing draw ratio. For the curves of original (undrawn) samples, the peak begins to appear at 124.5 °C. Judging from in Figure 3a−e, it may be expected that no crystallization occurs.

A different tendency was confirmed for the specimens drawn at $\lambda = 2$ in a hot water bath. The crystallization begins at 115.1 °C as shown in Figure 5. This may be expected that the density fluctuation and crystallization occurs simultaneously above 115 °C (as shown in Figure 4).

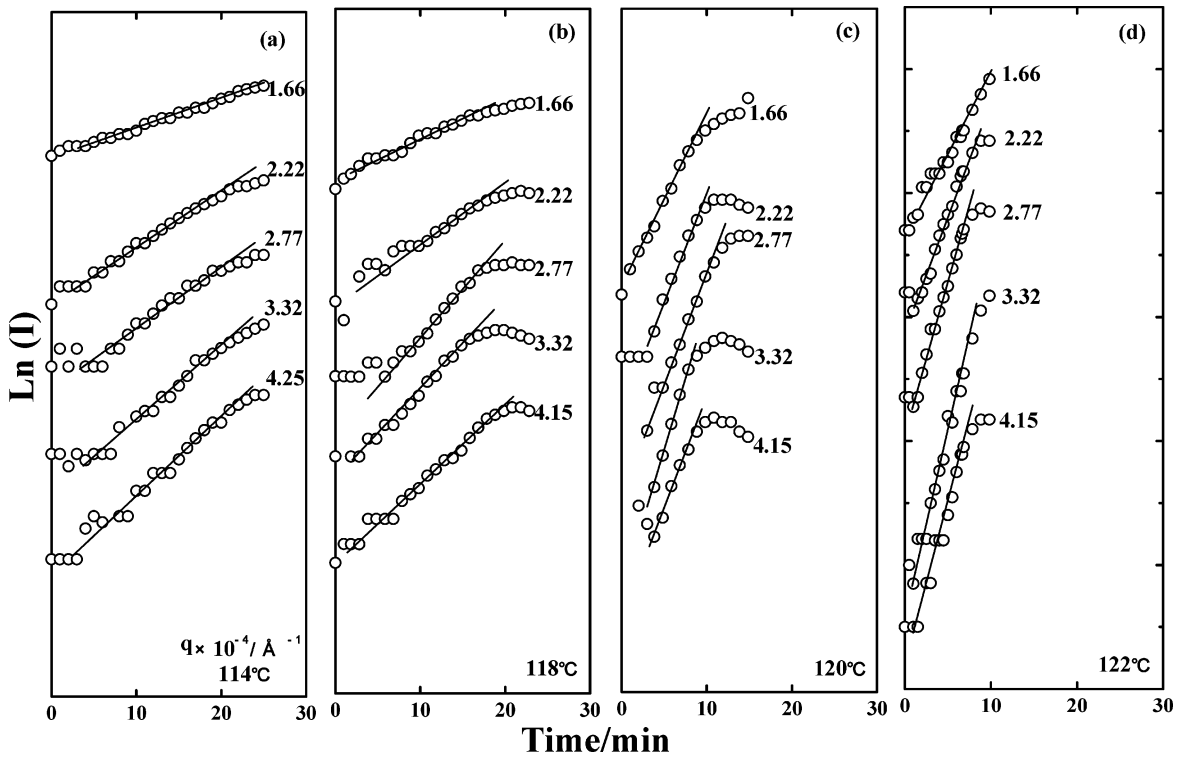

Figure 4. Logarithm plots of the scattered intensity against time at various q after the initiation of spinodal decomposition observed for PET films drawn to $\lambda = 2$ in a hot water bath at 100 °C. The specimens were annealed at the indicated temperature.

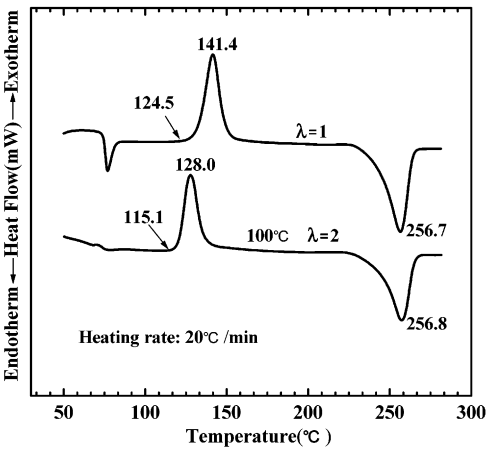

Figure 5. DSC profiles for PET films with different draw ratios drawn at the indicated temperature. The heating rate was 20 °C/min.

To facilitate an understanding for the detailed information for thermal crystallization, the X-ray intensity distribution was measured as a function of time at fixed temperature. Parts a and b of Figure 6 show the change in WAXD intensity profiles for the undrawn specimens ($\lambda = 1$) under annealing process at 114 °C and the specimen with $\lambda = 2$ under annealing process at 120 °C, respectively. For convenience, each curve is represented by shifting along the intensity axis to make a clear time dependence of the intensity distribution. The time described in the two diagrams indicates the beginning time of the accumulation of the X-ray intensity. The accumulation times were 5 and 2 min for undrawn ($\lambda = 1$) and drawn ($\lambda = 2$) films, respectively. For the undrawn specimen, the intensity distribution curve at 0 min denotes the accumulation intensity in the range from 0 to 5 min, since the accumulation time is 5 min. Accordingly, 0−5 and 15−20 min correspond to stage I, 25−30 and 40−45 min correspond to stage II, 56−61 min corresponding to the intermediate stage from the end of stage II to stage III, and 60−65 and 76−81 min correspond to stage III (as shown in Figure 1). In stage I and stage II, the X-ray intensity diffraction still shows a smooth curve with a maximum around $\theta_B = 21°$ (θ_B: Bragg angle), which is attributed to the scattering from amorphous regions. Beyond 54 min in Figure 6a, the X-ray intensity distribution shows that the sample starts to crystallize; the halo begins to split into several very weak, dim diffraction peaks. This means that stage II ensuring the linear relationship of ln(I) against time is independent of crystallization because of no existence of crystallites detected by X-ray diffraction. A similar tendency was observed for the specimen annealed at 118 °C.

The X-ray diffraction was also measured for the specimen with $\lambda = 2$ under the annealing process at 120 °C. The indication "8 min" corresponds to 0−2 min in Figure 4c. The intensity from the specimen with $\lambda = 2$ shows the reflection from the (010), (100), and ($\bar{1}$10) planes, when annealing time is beyond 8 min, which indicates that the progression of crystallization. Of course, the reflection from the crystal planes was detected at 8 min (corresponding to 0−2 min in Figure 4a) under the annealing process at 120 °C. This indicates that for the drawn film ($\lambda = 2$) the stage II ensuring the linear relationship in Figure 4 is associated with the simultaneous occurrence of density fluctuation and crystallization.

Figure 7a shows the change in ln(I) at $q = 2.77 \times 10^{-4}$ Å and the appearance of the small angle light scattering under H_v polarization condition against time measured for the undrawn film ($\lambda = 1$). Figure 7b shows the density dependence against time and the corresponding crystallinity calculated by eq 1 assuming the intrinsic densities of the crystal and amorphous phases as described in the Experimental Section. The sample

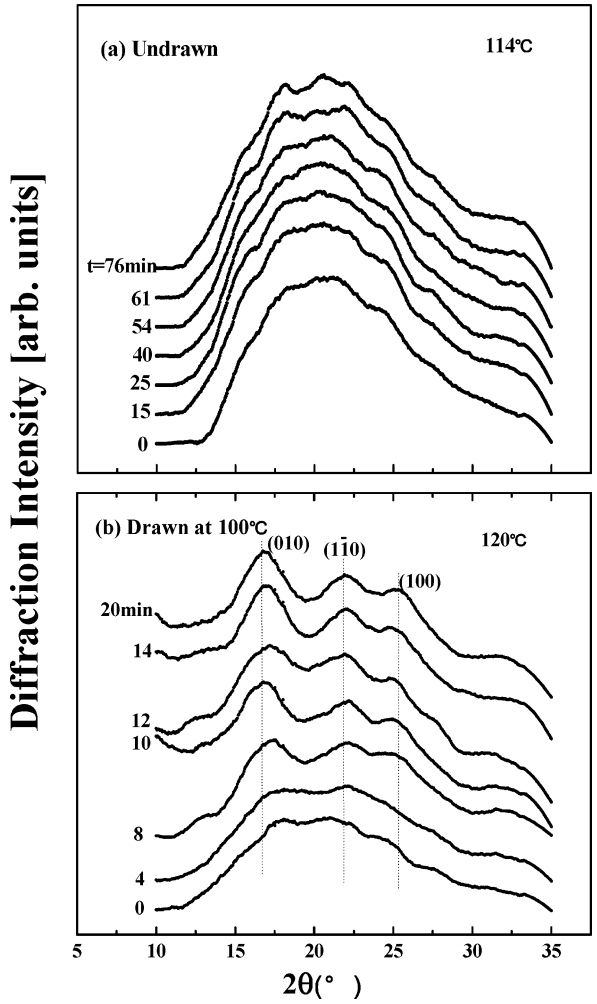

Figure 6. Change of WAXD profiles with time. The samples were isothermally annealed at the indicated temperature.

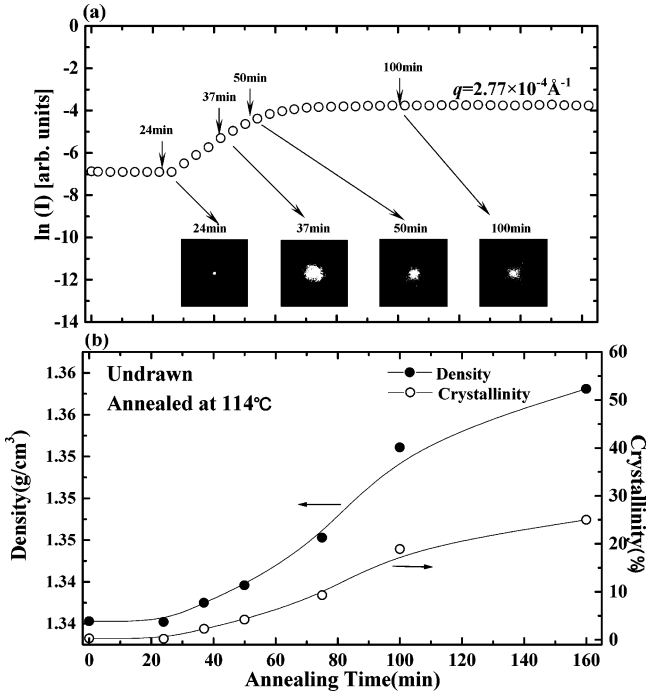

Figure 7. (a) Change of ln(I) at $q = 2.77 \times 10^{-4}$ Å^{-1} and the H_v SALS patterns with time. (b) Annealing time dependence of the density and the crystallinity of undrawn amorphous PET.

was heated rapidly to 114 °C and kept at the same temperature. As shown in Figure 7a, H_v scattering does not appear in stage I, indicating no existence of superstructure detected at the wavelength level of a He−Ne gas laser. In stage II, H_v scattering showed an indistinct pattern. Such a pattern has been reported to be due to scattering from sheaflike structures[28] with large fluctuation of optical axes. In the sheaflike structures, the optical axes correspond to the ordered aggregation of amorphous chains. Actually, the apparent crystallinity was about 5%, and any X-ray diffraction peak from the crystal plane could not be observed in stage I and stage II, as shown in Figure 6a. In other words, no rapid increase in density occurs in stages I and II. At 100 min in stage III, the pattern becomes clearer, indicating the growth of crystallization (ca. 20% crystallinity) within the sheaflike texture.

Similar measurements were done for the drawn film ($\lambda = 2$). Figure 8 shows the results. H_v scattering did not appear in stage I. But an indistinct pattern appeared at the starting time of stage II, and with increasing time, the pattern becomes clearer and provides four-leaf clover type indicating the existence of spherulites. With further lapse of time, the pattern becomes more distinct, indicating an increase in the number of spherulites associated with gradual development of crystallites. Of course, the density of the drawn film increases drastically in stage II, as shown in Figure 8b.

Figure 9 shows the evolution of scattered light intensity of the undrawn film plotted against q at the indicated times. The samples were heated rapidly at 110, 112, and 118 °C and kept at the same temperature. The arrow indicates the onset of stage II. In stage I (ca. 0−60 min for the sample annealed at 110 °C, ca. 0−34 min for the sample annealed at 112 °C and ca. 0−14 min for the sample annealed at 118 °C), the very weak scattered intensity hardly increases. This means that the sizes of domains with higher density produced by density fluctuation are much smaller than the wavelength of the used light.

On stage II (ca. 60−120 min for the sample annealed at 110 °C, ca. 34−82 min for the sample annealed at 112 °C, and ca. 14−28 min for the sample annealed at 118 °C), the scattered intensity begins to increase linearly depending on q, indicating that the size of ordered amorphous domains become comparable to the q range. At 110 °C, the scattered intensity decreases monotonically with increasing q. On the other hand, a scattering peak was observed for the specimens annealed at 112 and 118 °C. The scattering peak becomes higher with increasing time, but the peak is at the same position.

In stage III, the scattering peak tends to decrease with annealing time, but regretfully the exact peak position cannot be determined because of the limitation of our diffractmeter. Namely, our instrument cannot provide continuous intensity change as a function of q, since the setting angles of photodetectors are 2° intervals like 4°, 6°, 8°, 10°, ... Thus, we cannot examine the behavior of the scattering profiles in stage III in terms of Furukawa's scaling theory[29,30] although Imai et al. have done SAXS profiles of PET.[25]

The scattered intensity after annealing for more than ca. 90 min at 112 °C and that after annealing for more than ca. 36 min at 118 °C exhibits no scattering peak in the observed q range; the scattering peak may shift

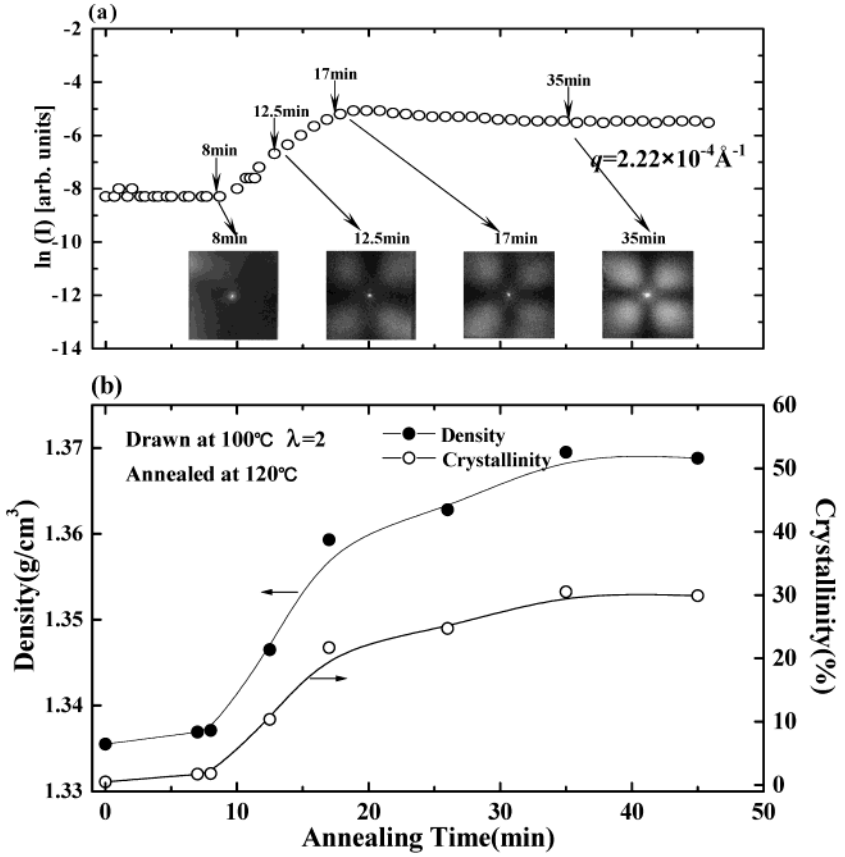

Figure 8. (a) Change of ln(I) at $q = 2.22 \times 10^{-4}$ Å^{-1} and the H_v SALS patterns with time. (b) Annealing time dependence of the density and crystallinity of the specimens drawn to $\lambda = 2$ in a hot water bath at 100 °C.

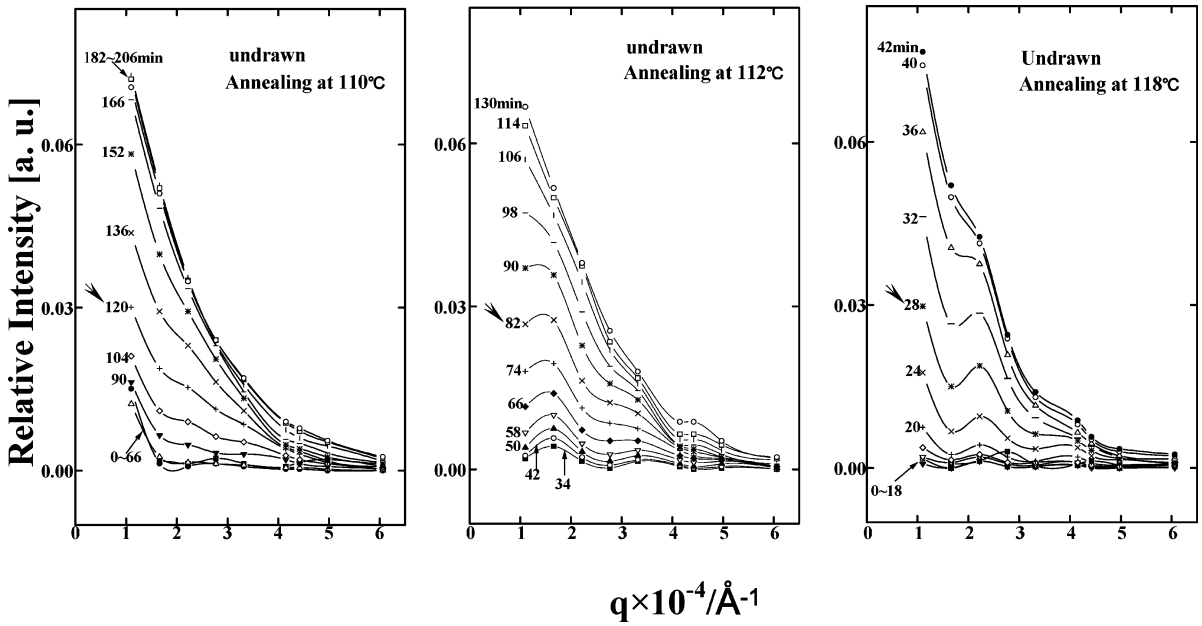

Figure 9. Change of the scattering intensity profiles with time for undrawn amorphous PET films annealing at the indicated temperature.

to lower scattering angle than the observable limit. Of course, the crystallites at 114 °C could not be detected in stage II by X-ray diffraction as discussed already. Accordingly, this is surely thought to be due to one of the characteristic phenomena, as have been reported for the phase separation of amorphous blend by spinodal decomposition. In the precrystallization stage, it may be expected that the mobility of amorphous chains provides phase separation of amorphous phase to dissolve thermodynamic unstable state and yields high and poor density regions. With an increase in annealing temperature, the peak slightly shifted toward higher q. For the scattering peak, the periodic structure characterizing spinodal decomposition can be estimated to be ca. 3.8 μm for the sample annealed at 112 °C and ca. 2.8 μm for the sample annealed at 118 °C.

As discussed already, no crystallite detected by X-ray measurements appears for the undrawn film ($\lambda = 1$) in

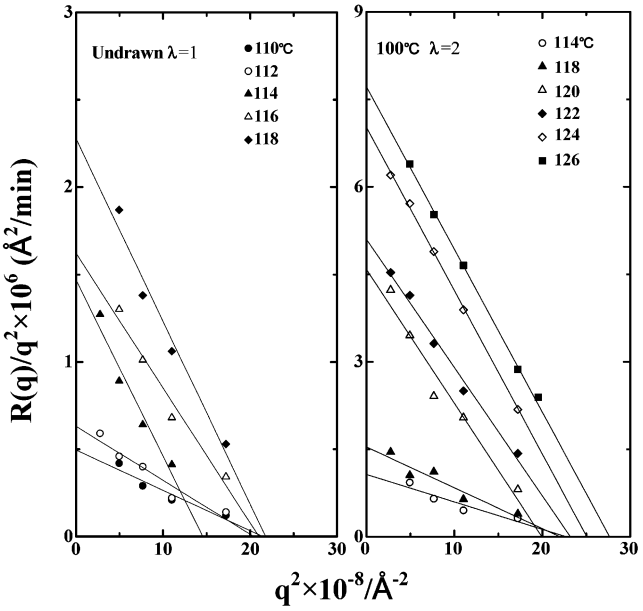

Figure 10. Plot of $R(q)/q^2$ vs q^2 for PET films at different isothermal temperature. The data were analyzed in the linear SD regime.

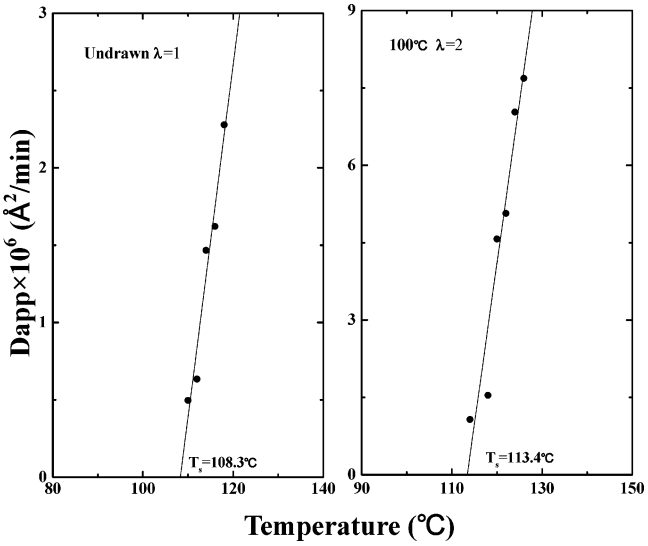

Figure 11. Temperature dependence of $D_{app} = R(q)/q^2|_{q=0}$ from which the spinodal temperature T_s is deduced. The data were analyzed in the linear SD regime for PET film.

the stage II. However, for the drawn film ($\lambda = 2$), the density fluctuation and crystallization occuring simultaneously above the spinodal temperature (as will be clarified in the following discussion) indicated a continuous transition from the amorphous to the partially crystalline state.[13] Accordingly, the linear increase in the logarithm of the scattered intensity against time is thought to be due to the possibility of successful analysis of the linear theory of spinodal decomposition proposed by Chan.[26,27] The deviation of the linear relationship is similar to the later stage of spinodal decomposition as has been observed for amorphous blends.[22] The deviation shifts to shorter time scale as the temperature increase and further the larger the q values and the earlier the stage where the deviation starts.[22]

If the linear relationship reflects the initial stage of spinodal decomposition as pointed by Cahn,[27] it is well-known that the change in scattered intensity in Figures 3 and 4 can be given by

$$I(q,t) = I(q,t=0) \exp[2R(q)t] \tag{2}$$

where $I(q,t)$ is the scattered intensity at the time t, after initiation of the spinodal decomposition, and $R(q)$ is the growth rate of density fluctuation given as a function of q; $R(q)$ is given by

$$R(q) = -D_c q^2\{\partial^2 f/\partial\rho^2 + 2\kappa q^2\} \tag{3}$$

where D_c is the translational diffusion coefficient of the amorphous chains in the PET film, f is the free energy, ρ is the density of the PET film, and κ is the density-gradient energy coefficient defined by Cahn and Hilliard.[26,27] A linear relationship in the plots of $\ln(I)$ vs t at fixed q was also confirmed as shown in Figures 3 and 4.

To give more conclusive evidence for spinodal decomposition for the linear relationship, the spinodal temperature T_s was estimated according to the linear Cahn theory.[26,27] The analysis details were described elsewhere.[29]

Figure 10 shows plots of $R(q)/q^2$ vs q^2 based upon the linear theory. The specimens were annealed at the indicated temperature. A good linear relationship was obtained experimentally, indicating that the initial stage of phase separation can be described within the framework of the linear theory with good accuracy. The apparent diffusion coefficient D_{app}, defined by $D_{app} = -D_c(\partial^2 f/\partial\rho^2)$, can obtained by the intercept on the vertical axis.

Figure 11 shows the temperature dependence of D_{app}. A fairly good linear relationship was also obtained. From the intercept on the temperature axis, one can define the spinodal temperature T_s at $D_{app} = 0$.

Table 2 summarizes the characteristic parameters describing dynamics of phase separation. Among them, the values of D_{app} ($= -D_c(\partial^2 f/\partial c^2)$) are significant, which are efficiently estimated by obtaining an intercept at $q^2 = 0$ in the plot $R(q)/q^2$ vs q^2 by assuming pure spinodal decomposition. Because of the positive values of D_c by definition, the values of $\partial^2 f/\partial c^2$ take a negative value characterizing unstable regions, leading to spinodal decomposition. The small values of $\partial^2 R(q)/\partial q^2|_{q=q_m}$, hence $D_{app}(\partial^2 R(q)/\partial q^2|_{q=q_m} = 8D_{app})$, indicate no appearance of a scattering maximum of intensity at the initial stage of spinodal decomposition. To observe a distinct scattering maximum in the linear spinodal decomposition regime, it is evident that the value of D_{app} must be usually 2 or 3 orders of magnitude greater.

Figure 12 shows the growth rate of density $R(q)$ plotted against q. The maximum growth rate $R(q_m)$ of density fluctuation increases with increasing annealing temperature. The value of the scattering vector, q_m, shifts slightly toward higher value of q with increasing difference ($T_s - T$) between the annealing temperature, T, and spinodal temperature, T_s. This phenomenon satisfies the principle of spinodal decomposition for amorphous polymer solutions proposed by van Aartsen.[23] According to his theory, the value of q_m increases with increasing difference ($T_s - T$), if the range of molecular interaction associated with the mean-square radius of gyration based on the concept of Debye et al.[30] is independent of temperature. Thus, the shift of $R(q_m)$ to a higher value of q on increasing the difference ($T_s - T$) justified the earlier conclusion that the linear theory

Table 2. Characteristic Parameters of Spinodal Decomposition of PET Film[a]

sample	temp (°C)	$q_m \times 10^{-4}$ (Å^{-1})	$q_c \times 10^{-4}$ (Å^{-1})	$\Lambda_m \times 10^{-4}$ (Å)	Λ_c (Å)	$R(q_m)$ (min^{-1})	$D_{app} \times 10^6$ (Å^2/min)
undrawn, $\lambda = 1$	110	3.27	4.63	1.92	1.36	0.027	0.5
	112	3.20	4.52	1.96	1.39	0.032	0.63
	114	2.70	3.82	2.33	1.64	0.054	1.47
	116	3.24	4.58	1.94	1.37	0.085	1.62
	118	3.30	4.66	1.90	1.35	0.124	2.28
100 °C, $\lambda = 2$	114	3.35	4.74	1.87	1.32	0.06	1.07
	118	3.32	4.69	1.89	1.34	0.08	1.54
	120	3.17	4.48	1.98	1.4	0.23	4.57
	122	3.41	4.82	1.84	1.3	0.29	5.07
	124	3.54	5.00	1.77	1.26	0.44	7.03
	126	3.74	5.29	1.68	1.19	0.54	7.69

[a] Data are obtained from the plots of $R(q)/q^2$ vs q^2. q_c: the "maximum wavenumber" of fluctuation that can grow from the intercept of q^2 at which $R(q)/q^2 = 0$. q_m: the "most probable wavenumber" of fluctuation that can grow at the highest rate, being estimated from q_c ($q_m = q_c/2^{1/2}$). $\Lambda_m = 2\pi/q_m$, $\Lambda_c = 2\pi/q_c$.

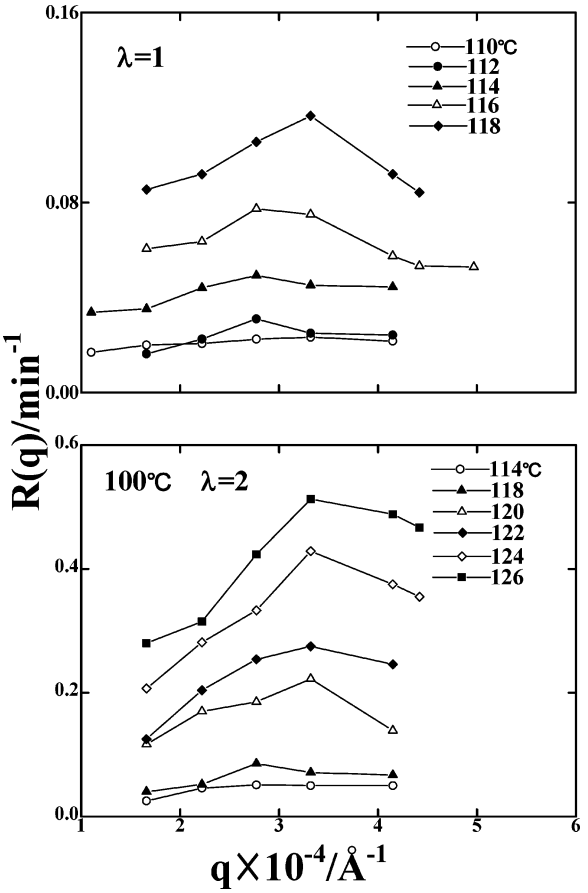

Figure 12. Growth rate of density fluctuation $R(q)$ plotted against q for the PET films with different ratios drawn at the indicated temperature.

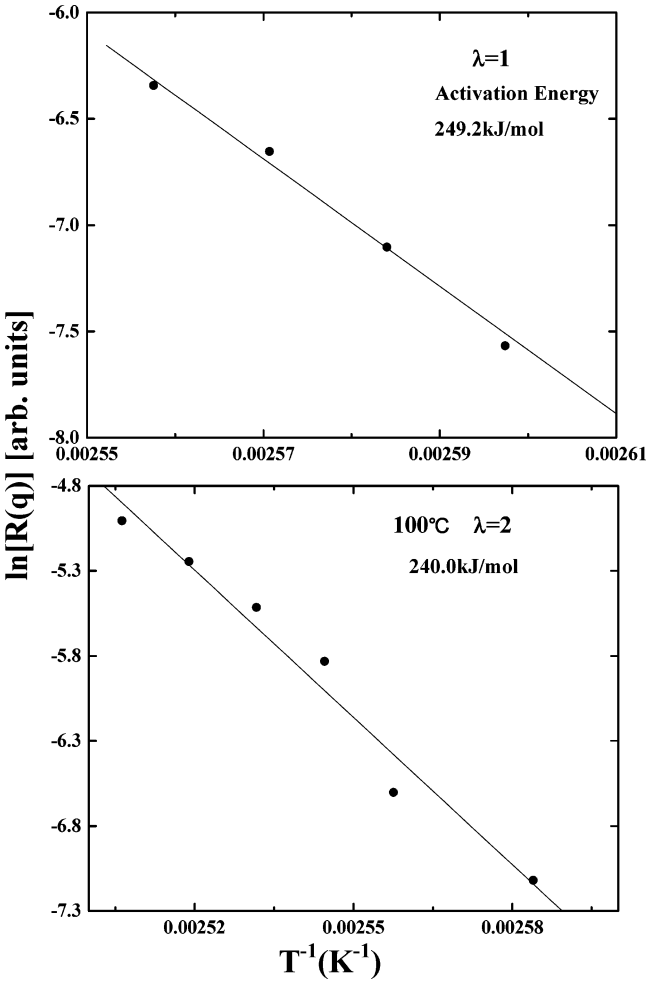

Figure 13. Annealing temperature dependence of the logarithm of the growth rate $R(q)$ at $q = 2.77 \times 10^{-4}$ Å^{-1}. The data were obtained in the linear SD regime (stage II).

of the spinodal decomposition proposed by van Aartsen[23] and the theory of Cahn et al.[26,27] can be applied to density fluctuation of amorphous PET chains by rapid temperature jump. In other words, eq 2 associated with the linear Cahn theory is applicable for the analysis of the linear relationship of ln(I) vs time in Figures 3 and 4.

Following Cahn's theory,[26,27] the concentration fluctuation relating to eq 1 at the proper long time t can be rewritten approximately as follows:

$$\langle|\rho(q,t) - \rho_0|^2\rangle \approx \langle|\rho(q_m,t) - \rho_0|^2\rangle \propto \exp[2R_m(q_m)t] \quad (4)$$

where $|\rho(q,t) - \rho_0|$ is the density fluctuation at t. Equation 4 suggests the existence of a scattering peak at θ_m from $q_m = (4\pi n/\lambda)\sin(\theta_m/2)$. Actually, the scattering peak has been observed at the later stage of spinodal decomposition for amorphous blend films.[33] No appearance of the scattering peak at the later stage of phase separation of amorphous PET chains is thought to be due to the very broad curve of $R(q)$ against q.

Here we must emphasize that the scattered intensity with time as shown in Figures 3 and 4 increased very slowly and nonexponentially when the specimens with $\lambda = 1$ and 2 were annealed immediately at $T < T_s$ by rapid-temperature jump. No peak was observed in the plots of $R(q)$ against q and no scattering maximum appears. Also, an increase in density could not be confirmed within experimental error. This indicates that

density fluctuation does not occur at temperatures lower than spinodal temperature in the q range in this experiment. This justifies that the density fluctuation occurs as prestage of crystallization and the fluctuation can be analyzed by the initial stage of spinodal decomposition by Chan apparently.

Figure 13 shows annealing temperature dependence of the logarithm of the growth rate $R(q)$ at $q = 2.77 \times 10^{-4}$ Å. The data were obtained in the linear SD regime (stage II). A good linear relationship was obtained, indicating that the rate $R(q)$ corresponding to stage II (early stage of SD) can be described by an Arrhenius-type plot, which is given as

$$R(q) = R_0 \exp(-\Delta E/RT) \tag{5}$$

where R_0 is a coefficient, R is universal gas constant, and ΔE is the activation energy. Judging from the values, it is obvious that the activation energy decreases with increasing orientational degree of amorphous chain segments as listed in Table 1. This means that the crystallization of the drawn film is easier than that of the undrawn film because of the ordered arrangement of amorphous chains. In other words, freely jointed statistical segments with active mobility require more energy to crystallize. Anyway, the activation energy of stage II (the initial stage of SD) in the present experiment is slightly lower than that (296 kJ/mol) of the later stage of SD in the experiment by Matsuba reported for PET.[20]

Conclusion

The thermal behavior of amorphous PET film by rapid jump of temperature was investigated in terms of the density fluctuation of amrrphous chains by using depolarized light scattering techniques. The logarithm of scattered intensity from amorphous PET film increased linearly with time in the initial stage (stage II) of the density fluctuation when the specimen was annealed immediately at a constant temperature. This phenomenon could be analyzed within the framework of the linear theory of SD proposed by Cahn. Namely, the amorphous chains at elevated temperature are thermodynamically unstable and tend to incur density fluctuation. This concept provided the definition of a sort of spinodal temperature. During the annealing process, compact molecular aggregates may be formed, and these connect to the heterogeneous continuous region (high-density amorphous phase). For the undrawn sample, despite the ordering of molecules in the high-density phase, the behavior was independent of crystallization. Actually, no appearance of crystallites was confirmed by X-ray diffraction and density measurements. The ordering structure in the high-density phase, however, forms optically anisotropic sheaflike texture independent of crystallization. Such behavior was confirmed by SALS measurement under polarization conditions. For the drawn sample, the density fluctuation and crystallization occur simultaneously above the spinodal temperature. This indicates a continuous transition from amorphous to the partially crystalline state. Of course, the scattered intensity with time increased very slowly and nonexponentially in stage II; no peak was observed in the plots of $R(q)$ against q, and no scattering maximum appears when the specimen was heated by rapid jump up to temperatures lower than spinodal temperature. Also, any increase in density could not be confirmed within the experimental error.

References and Notes

(1) Gilmer, J. W.; Wiswe, D.; Zachmann, H. G. *Polymer* **1986**, *27*, 1391.
(2) Gehrhe, R.; Reikel, C.; Zachmann, H. G. *Polymer* **1989**, *30*, 1582.
(3) Middleton, A. C.; Duckett, R. A. *J. Appl. Polym. Sci.* **2001**, *79*, 1825.
(4) Radhakrishnan, J.; Kaito, A. *Polymer* **2001**, *42*, 3859.
(5) Asano, T.; Baltá Calleja, F. J. *Polymer* **1999**, *40*, 6475.
(6) Imai, M.; Kaji, K. *Phys. Rev. Lett.* **1993**, *71*, 4162.
(7) Imai, M. *Phys. Rev. B* **1995**, *52*, 12696.
(8) Imaim, M. *Phys. Rev. Lett.* **1993**, *71*, 4162.
(9) Geil, P. H. In *Order in the Amorphous State of Polymers*; Keinath, S. E., Miller, R. L., Rieke, J. K., Eds.; Plenum: New York, 1987.
(10) Herglotz, H. K. *J. Colloid Interface Sci.* **1980**, *75*, 105.
(11) Doi, M.; Shimada, T.; Okano, K. *J. Chem. Phys.* **1988**, *88*, 4070.
(12) Terril, N. J.; Fairclough, P. A. *Polymer* **1998**, *39*, 2381.
(13) Strobl, G. R. *The Physics of Polymers*, 2nd ed.; Berlin: Springer, 1997; p 173.
(14) Strobl, G. R. *Trends in Non-Crystalline Solid*; Conde, A., Conde, C. F., Millan, M., Eds.; World Scientific: Singapore, 1992; p 37.
(15) Brandrup, J.; Immergut, E. H.; Grulke, E. A. *Polymer Handbook*, 4th ed.; John Wiley & Sons: New York, 1999.
(16) Yang, H.; Shibayama, M.; Stein, R. S.; Shimizu, N.; Hashimoto, T. *Macromolecules* **1986**, *19*, 1667.
(17) Wallach, M. L. *J. Polym. Sci., Part C* **1966**, *13*, 69.
(18) Shimada, T.; Doi, M.; Okano, K. *J. Chem. Phys.* **1988**, *88*, 7181.
(19) Tadokoro, H. *Structure of Crystalline Polymers*; Wiley: New York, 1978.
(20) Matsuba, G.; Kaji, K. *Phys. Rev. E* **2002**, *65*, 061801.
(21) Matsuba, G.; Kanaya, T.; Kaji, K.; Nishida, K. *Abstract of IUPAC Macro 2000*; Wiley-VCH: Berlin, 2000.
(22) Hashimoto, T.; Kumaki, J.; Kawai, H. *Macromolecules* **1983**, *16*, 641.
(23) van Aartsen, J. J. *Eur. Polym. J.* **1970**, *6*, 919.
(24) Imai, M.; Mori, K.; Mizukami, T. *Polymer* **1992**, *33*, 4451.
(25) Imai, M.; Mori, K.; Mizukami, T. *Polymer* **1992**, *33*, 4457.
(26) Cahn, J. W. *J. Chem. Phys.* **1965**, *42*, 93.
(27) Cahn, J. W.; Hilliard, J. E. *J. Chem. Phys.* **1958**, *28*, 258.
(28) Matsuo, M.; Tamada, M.; Terada, T.; Sawatari, C.; Niwa, M. *Macromolecules* **1982**, *15*, 988.
(29) Furukawa, H. *Physical* **1984**, *123A*, 497.
(30) Furukawa, H. *Adv. Phys.* **1985**, *34*, 703.
(31) Matsuo, M.; Kawase, M.; Sugiura, Y.; Takematsu, S.; Hara, C. *Macromolecules* **1993**, *26*, 4461.
(32) Debye, P. *J. Chem. Phys.* **1959**, *31*, 680.
(33) Middleton, A. C.; Duckett, R. A. *J. Appl. Polym. Sci.* **2001**, *79*, 1825.

MA030408R